SCIENTIFIC REPORTS

OPEN

SUBJECT AREAS:
ELECTRONIC AND SPINTRONIC DEVICES
PHOTONIC DEVICES

Received
30 January 2014

Accepted
7 May 2014

Published
28 May 2014

Correspondence and requests for materials should be addressed to G.F.X. (gfxie@xtu.edu.cn) or G.Z. (zhangg@ihpc.a-star.edu.sg)

A Bond-order Theory on the Phonon Scattering by Vacancies in Two-dimensional Materials

Guofeng Xie[1], Yulu Shen[1], Xiaolin Wei[1], Liwen Yang[1], Huaping Xiao[1], Jianxin Zhong[1] & Gang Zhang[2]

[1]Hunan Key Laboratory of Micro-Nano Energy Materials and Devices, Faculty of Materials, Optoelectronics and Physics, Xiangtan University, Hunan 411105, P.R. China, [2]Institute of High Performance Computing, Singapore 138632, Singapore.

We theoretically investigate the phonon scattering by vacancies, including the impacts of missing mass and linkages (τ_V^{-1}) and the variation of the force constant of bonds associated with vacancies (τ_A^{-1}) by the bond-order-length-strength correlation mechanism. We find that in bulk crystals, the phonon scattering rate due to change of force constant τ_A^{-1} is about three orders of magnitude lower than that due to missing mass and linkages τ_V^{-1}. In contrast to the negligible τ_A^{-1} in bulk materials, τ_A^{-1} in two-dimensional materials can be 3–10 folds larger than τ_V^{-1}. Incorporating this phonon scattering mechanism to the Boltzmann transport equation derives that the thermal conductivity of vacancy defective graphene is severely reduced even for very low vacancy density. High-frequency phonon contribution to thermal conductivity reduces substantially. Our findings are helpful not only to understand the severe suppression of thermal conductivity by vacancies, but also to manipulate thermal conductivity in two-dimensional materials by phononic engineering.

Thermal property of two-dimensional materials has attracted considerable attention due to the unique physical attributes[1–4] and the potential applications[5–8] in many areas. On the one side, because of its superior high thermal conductivity, graphene-based devices can be applied in nanoscale phononics and for thermal management[9–16]. On the other side, the ultra low thermal conductivity of monolayer molybdenum disulfide (MoS_2) sheet and nanoribbon[17–19] opens up the possibility to realize two-dimensional thermoelectric devices based on Transition metal dichalcogenides (TMD) materials for heat energy harvesting and refrigeration. Most materials have natural point defects, such as atomic vacancies introduced in the process of fabrication. Since the phonon frequency depends on length and energy of the local bonds[20], these vacancy defects offer a possibility for tailoring the thermal conductivity of materials[21–25].

Phonon scattering by vacancies in crystals was originally treated from perturbation theory by Ratsifaritana and Klemens. Although the role of the strain field in scattering of phonons is important since strain would change the local value of phonon frequency for a fixed wave vector, thus contributing to the perturbation, Ratsifaritana and Klemens demonstrated that the distortion effects could be neglected for vacancies, and the perturbation of vacancy defect was one that corresponds to the removal of the mass of one atom and the force constants of two atoms[26]. In addition to the missing mass and missing linkages (τ_V^{-1}), the change of force constant of bonds between the under-coordinated atoms near the vacancies also results in phonon scattering (τ_A^{-1}), but it is neglected in the theoretical model of vacancy. Usually, the interatomic force constants can be obtained by the quantum chemistry calculations. However, it is not reliable to investigate the vacancy effect on phonon scattering in sizeable materials due to computational limitation.

In this communication, we report our findings on the phonons scattering (both τ_V^{-1} and τ_A^{-1}) by vacancies, including the impacts of missing mass, missing linkages, and change of force constant of the under-coordinated atoms near the vacancies based on the frame work of bond-order-length-strength (BOLS) notation[27,28]. We find that the phonon scattering rate due to change of force constant τ_A^{-1} is about three orders of magnitude less than that due to missing mass and linkages τ_V^{-1} in bulk crystals. In contrast to the negligible τ_A^{-1} in the bulk, τ_A^{-1} in two-dimensional materials can be 3–10 folds larger than τ_V^{-1}. The critically different phonon scattering rate determines that in two-dimensional materials with vacancies, the contribution to thermal conductivity from high frequency phonons is greatly suppressed. Consistency in the present and molecular dynamics simulations[29] on the thermal conductivity of defected single-layer graphene confirmed our expectations.

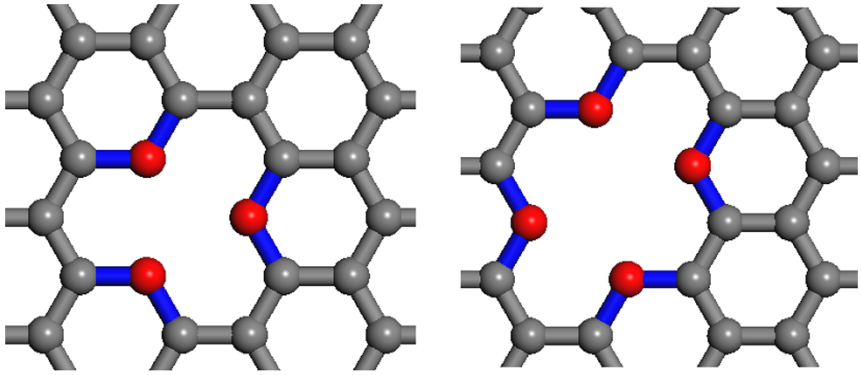

Figure 1 | Schematic description of graphene flakes with (a) single vacancy. The CN of carbon atoms in graphene is 3. There are 3 under-coordinated atoms displayed as red colour whose CN is 2 near the single vacancy, and bonds displayed as blue colour between the under-coordinated atoms near the vacancy become stronger. (b) double vacancy.

Results

Bond-order theory for phonon-vacancy scattering. Perturbation theory in terms of the missing mass and the missing linkages deals with the scattering of phonons by vacancy defects in crystals[26,30],

$$\tau_V^{-1} = x\left(\frac{\Delta M}{M}\right)^2 \frac{\pi}{2}\frac{\omega^2 g(\omega)}{G} \tag{1}$$

where x is the density of vacancies, G is the number of atoms in the crystal, $g(\omega)$ is the phonon density of states (DOS). For vacancy defect, the effective value of $\frac{\Delta M}{M}$ is $-\frac{M_a}{M}-2$, where M is the average mass per atom, M_a is the mass of the missing atom, and the term -2 accounts for the potential energy of the missing linkages, or twice the potential energy per atom[26,31].

One important fact that has been overlooked in previous modeling is that bond between under-coordinated atoms becomes shorter and stronger[28]. Bond shortening and strengthening not only raises the local density of charge, mass and energy but also deepens the local potential, providing perturbation to the local potential. This under-coordination effect raises the local energy density, or the elastic modulus, and subsequently the trap for phonon and electron transportation[32,33]. The coordination number (CN) dependence of bond-contraction coefficient (C_z) and bond energy (E_z) follow the relation[28],

$$\begin{cases} C_z = d_z/d_0 = 2/\{1+\exp[(12-z)/(8z)]\} & \text{(bond}-\text{contraction coefficient)} \\ E_z = C_z^{-m} E_b & \text{(Single}-\text{bond}-\text{energy)} \end{cases} \tag{2}$$

where z is the effective coordination number, d_z is the bond length. In BOLS theory, the effective CN for bulk materials is always 12, regardless of the nature of the bond or the crystal configuration[34], E_b and d_0 are the corresponding bulk values of single bond energy and bond length, respectively. m is an indicator for bond nature of a specific material, which is not freely adjustable. For alloys and compounds (such as MoS_2 and BN) m is around 4, for C and Si the value of m has been optimized to be 2.56 and 4.88, respectively[35].

Eq. (2) yields the change of force constant of bonds between under-coordinated atoms, from the perspective of dimensionality analysis[28],

$$k_z = d^2u(r)/dr^2\big|_{r=d_z} \propto E_z/d_z^2 \tag{3}$$

Accordingly, the bond force constant nearby the vacancies increases compared with that far away from vacancies. As shown in Fig. 1 (the schematic description of graphene flakes with single and double vacancy), the bonds displayed as blue colour between the under-coordinated atoms near the vacancy become stronger. According to the perturbation theory of Klemens, the rate of phonon scattering by atoms of different force constant is given as[36,37],

$$\tau_A^{-1} = x\left(\frac{\delta k}{k}\right)^2 4\pi \frac{\omega^2 g(\omega)}{G} \tag{4}$$

where x is the density of imperfections, k is the force constant, and δk is the change of force constant.

According to Eq. (2) and Eq. (3), we can get

$$\begin{aligned} \frac{k_{z-1}}{k_z} &= \frac{E_{z-1}d_z^2}{E_z d_{z-1}^2} = \left(\frac{C_{z-1}}{C_z}\right)^{-(m+2)} \\ &= \left\{\frac{1+\exp[(12-z)/(8z)]}{1+\exp[(13-z)/(8z-8)]}\right\}^{-(m+2)} \end{aligned} \tag{5}$$

where k_{z-1} is the force constant of under-coordinated atoms near the vacancies whose CN is z-1, and k_z is the force constant of atom whose CN is z. Therefore, according to Eq. (4) and Eq. (5), the scattering rate of phonons by the under-coordinated atoms near the vacancies is derived as,

$$\begin{aligned} \tau_A^{-1} &= x_A\left(\frac{k_{z-1}}{k_z}-1\right)^2 4\pi\frac{\omega^2 g(\omega)}{G} \\ &= 4\pi z x\left\{\left[\frac{1+\exp[(12-z)/(8z)]}{1+\exp[(13-z)/(8z-8)]}\right]^{-(m+2)}-1\right\}^2 \frac{\omega^2 g(\omega)}{G} \end{aligned} \tag{6}$$

where $x_A = zx$ is the density of the under-coordinated atoms, and x is the density of single vacancy. m is a key parameter that represents the nature of the bond.

The unusual vacancy effects on phonon scattering in 2D materials. The ratio of τ_A^{-1} to τ_V^{-1} in the case of different m and different coordination number is shown in Fig. 2. For bulk materials whose effective atomic CN is always 12 in the BOLS correlation mechanism, τ_A^{-1} is three orders of magnitude less than τ_V^{-1}, so the scattering of phonons by the under-coordinated atoms near the vacancies is negligible in bulk materials. The ratio τ_A^{-1}/τ_V^{-1} increases quickly with decreasing the coordination number. For two-dimensional materials with $z = 3$, such as silicene, hexagonal Boron Nitride, graphene and MoS_2, τ_A^{-1} is 3- to 10-fold larger than τ_V^{-1}, therefore the scattering of phonons by the under-coordinated atoms near the vacancies must be taken into account, and the total scattering rate of phonons by the imperfections should be $\tau_V^{-1}+\tau_A^{-1}$.

Moreover, the ratio τ_A^{-1}/τ_V^{-1} increases with the parameter m increases. For carbon-based 2D materials, that is, graphene, m is

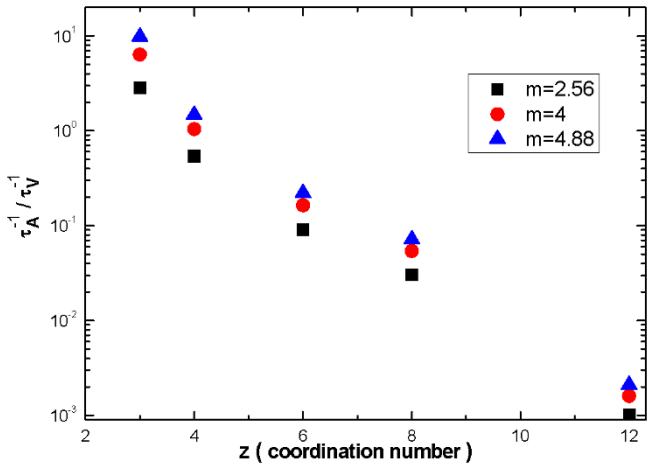

Figure 2 | The ratio of τ_A^{-1} to τ_V^{-1} in the case of different *m* and different CN. Coordination number $z = 12$ represents the phonon scattering in bulk materials.

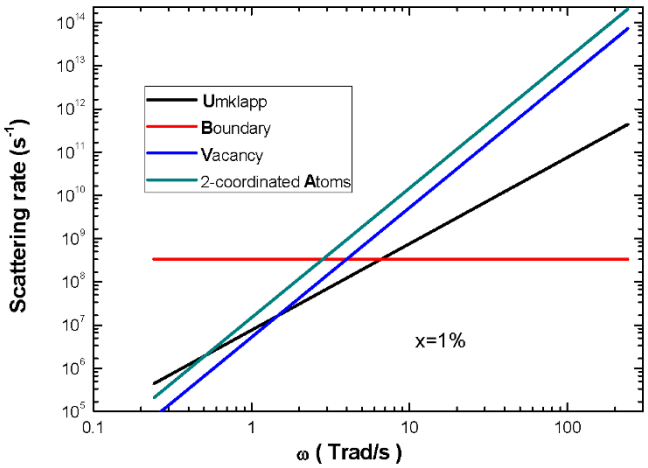

Figure 3 | The phonon scattering rate as a function of phonon angular frequency. The phonon scattering mechanisms including Umklapp, boundary, vacancy and under-coordinated atoms scattering are considered.

found to be 2.56. From Fig. 2, the ratio τ_A^{-1}/τ_V^{-1} is 2.8. For 2D alloys and compounds, such as BN and transition metal dichalcogenides (TMDs) materials, *m* is around 4, results to a high τ_A^{-1}/τ_V^{-1} ratio of 6.4. Very recently, monolayer MoS_2, a member of TMD family, have gained considerable interest. Thus for 2D TMDs materials, the phonon scattering by under-coordinated atoms is dominated over that by vacancy itself.

Vacancy effects on phonon scattering in graphene flakes. It is an important phononic engineering technique to modulate the thermal transport by phonons with different range of frequency[38]. Next using graphene flake as an example, we discuss the impacts of vacancies on phonon scattering rate and thermal conductivity contributed from phonons with different frequency. The Matthiessen's rule which assumes that different scattering mechanisms are independent is adopted, so the total phonon scattering rate τ_λ^{-1} in branch λ is given as:

$$\tau_\lambda^{-1} = \tau_{U,\lambda}^{-1} + \tau_{B,\lambda}^{-1} + \tau_{V,\lambda}^{-1} + \tau_{A,\lambda}^{-1} \tag{7}$$

The Umklapp phonon-phonon scattering rate ($\tau_{U,\lambda}^{-1}$) and the phonon-boundary scattering rate ($\tau_{B,\lambda}^{-1}$) are given as[39],

$$\tau_{U,\lambda}^{-1} = \frac{\gamma_\lambda^2 k_B T \omega^2}{M v_\lambda^2 \omega_{D,\lambda}} \tag{8}$$

$$\tau_{B,\lambda}^{-1} = \frac{v_{\lambda,x}}{W}\frac{1-P}{1+P} \tag{9}$$

where *M* is the mass of a graphene unit cell, γ_λ is the Grüneissen parameter, *W* is the width of graphene ribbon, $v_{\lambda,x}$ is the component of the phonon velocity in branch λ perpendicular to the longitudinal direction of graphene ribbon, and *P* is the specularity parameter, which is defined as the probability of phonon's specular reflection at the lateral boundaries. In order to fit the experimental thermal conductivity value of pristine graphene, we set the specular parameter as 0.8, and the width of graphene flake as 5 μm, which are consistent with Ref. 40 and Ref. 41. As the major concern of the present work are the mechanism of phonon scattering by vacancies and the reduction of thermal conductivity by vacancies, the values of specular parameter and flake width are fixed. The Grüneissen parameters for acoustic branches originate from the results of first-principles calculations in Ref. 42. Based on the linear dispersion for in-plane branches and quadratic dispersion for out-of-plane branch (see Eq. 16 in the section of Methods), the function for phonon DOS of graphene is,

$$g(\omega) = \begin{cases} \dfrac{S\omega}{2\pi v_\lambda^2} & \lambda = LA,\ TA \\ \dfrac{S}{4\pi\alpha} & \lambda = ZA \end{cases} \tag{10}$$

Therefore according to Eq. (1), the rate of phonon scattering by single vacancies is given as,

$$\tau_{V,\lambda}^{-1} = \begin{cases} 2.25x\Omega\dfrac{\omega^3}{v_\lambda^2} & \lambda = LA,\ TA \\ 1.125x\Omega\dfrac{\omega^2}{\alpha} & \lambda = ZA \end{cases} \tag{11}$$

where *x* is the density of vacancies, and Ω is the primitive cell area of graphene.

As shown in Fig. 1(a), the CN of carbon atoms in graphene is 3. There are 3 under-coordinated atoms whose CN is 2 near the single vacancy. Based on BOLS theory, the bond between the under-coordinated atoms becomes shorter and stronger. Girit *et al.*[43] discovered that breaking a C–C bond of the 2-coordinated carbon atoms near the monolayer-GNR vacancy required 7.50 eV per bond, that was 32% higher than the energy (5.67 eV/bond) required for breaking one bond between 3-coordinated carbon atoms in the interior of a suspended graphene sheet. The mechanical strength of graphene increases with the density of defects[44] (the reconstructed 5- and 7-atom rings forming the grain boundaries), because of the particular strength of the ring bonds and their elongation dynamics. These findings provide evidence for the BOLS prediction of the shorter and stronger bonds at vacancies. According to Eq. (5), the ratio of force constant of the 2-coordinated carbon atoms near the vacancy to that of the 3-coordinated carbon atoms is 2.03, and according to Eq. (6), the rate of phonon scattering by the 2-coordinated carbon atoms near the single vacancies is given as,

$$\tau_{A,\lambda}^{-1} = \begin{cases} 6.36x\Omega\dfrac{\omega^3}{v_\lambda^2} & \lambda = LA, TA \\ 3.18x\Omega\dfrac{\omega^2}{\alpha} & \lambda = ZA \end{cases} \tag{12}$$

From Eq. (12) and Eq. (11), we know that the phonon scattering by the under-coordinated atoms near the vacancy dominates over that by the vacancy in graphene.

In the pristine graphene sheet, the Umklapp phonon-phonon scattering is dominant at room temperature, but in the defective graphene, the situation is quite different. Fig. 3 presents the frequency-dependent scattering rate of LA phonons for all kinds of

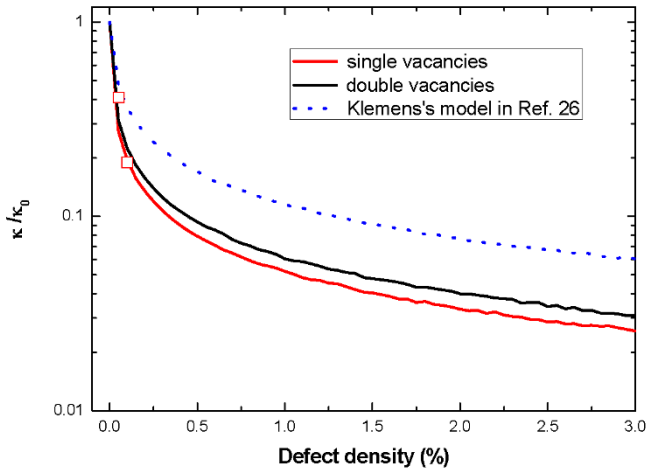

Figure 4 | The ratio of the thermal conductivity of defective graphene to the pristine one at room temperature as a function of defect density. The squares are the molecular dynamics simulation results of single vacancy defective graphene from Ref. 29.

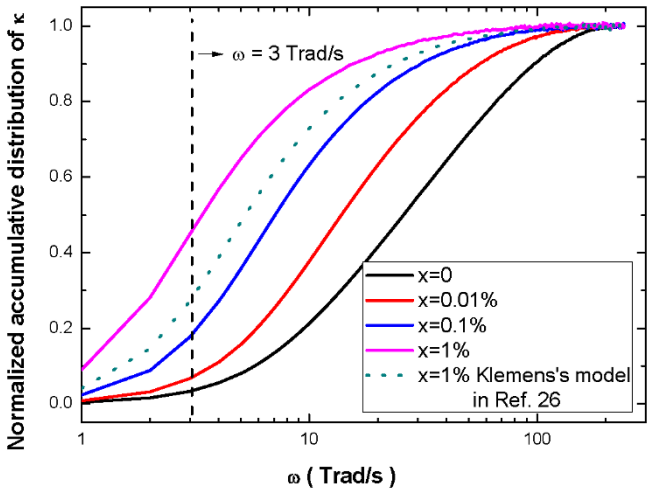

Figure 5 | The normalized accumulative distribution of thermal conductivity of graphene flakes as a function of phonon angular frequency. Here the width of graphene flake is 5 μm, concentrations of single-vacancy defect are 0%, 0.01%, 0.1%, and 1%, respectively. The solid lines are results from the present model. The dotted line is thermal conductivity of graphene flake with 1% vacancy calculated without considering the phonon scattering by under-coordinated atoms.

mechanisms in the single vacancy defective graphene. The vacancy density is 1%. For the ultra-low frequency phonons, the boundary scattering is dominant. However, for $\omega > 2.5$ *Trad/s*, the scattering by the under-coordinated carbon atoms dominates over other mechanisms. The situation is similar for other branches. However, this most important scattering mechanism is neglected in previous theoretical model on phonon scattering by vacancies.

Vacancy effects on thermal conductivity in graphene flakes. Many researches presented that the thermal conductivity of graphene could be remarkably reduced by point defects[22,29,45], such as isotope and vacancy. The vacancy effect on the thermal conductivity is more remarkable than that of isotope. By molecular dynamics simulation, Haskins *et al.* found that even for a very low vacancy concentration 0.1%, a 81% reduction of thermal conductivity of graphene was achieved[29]. Although Klemens's model agrees well with thermal conductivity reductions by vacancies in bulk materials[31,46], the severe suppression of thermal conductivity of graphene by vacancies is much over the prediction of Klemens's theory[22]. Incorporating phonon scattering by the under-coordinated atoms near the vacancies to the linearized phonon Boltzmann transport equation within relaxation time approximation (see in the section of Methods), we calculate the relative thermal conductivity (κ/κ_0) of defective graphene (single vacancies and double vacancies) as a function of defect density at room temperature, which is shown in Fig. 4. κ_0 (the thermal conductivity of pristine graphene) calculated by this work, 3750 W/mK, is coherent with various experimental measurements[47,48] and theoretical calculations[49,50]. The dash line is the calculation results by Klemens's model from Ref. 26, in which the phonon scattering by the under-coordinated carbon atoms near the vacancies is not considered. The solid lines are the results of the present model. The squares are the molecular dynamics simulation results of single vacancies in graphene from Ref. 29. It is obvious that the results predicted by the present model agrees better with molecular dynamics simulations than the results of Klemens's theory, and the phonon scatterings by the 2-coordinated carbon atoms near the vacancies further suppress the thermal conductivity of graphene.

Fig. 5 demonstrates the normalized accumulative distribution of thermal conductivity defined as Eq. (19) (see in the section of Methods) for different single vacancy density. The curves move towards the upper-left corner as the vacancy density increases. The ultra-low thermal conductivity of vacancy defective graphene stems from the significant suppression of high-frequency phonons. With the increasing of vacancy density, the contribution of more and more high-frequency phonons to heat conductance is severely suppressed by the scattering of the vacancies and the under-coordinated atoms near the vacancies, as shown in Fig. 5. From Fig. 3, we know that the scattering by these imperfections is dominant, except for the ultra-low frequency phonons. Therefore, the thermal conductivity of vacancy defective graphene is absolutely dominated by low-frequency acoustic phonons. For example, in the case of 1% concentration of single vacancy, the phonons of $\omega <$ 3 Trad/s have about 50% contribution to the thermal conductivity, which is shown in Fig. 5. However, in the Klemens's model (the dotted line), the same phonons only have about 30% contribution which is lower than our model, because it neglects additional scattering by the under-coordinated atoms near the vacancies.

Discussion

The theoretical model in present work can be used to explain the different content dependence in thermal conductivity of graphene flakes with single- and double-vacancy defects. For a single vacancy, there are 3 under-coordinated atoms around each defective atom, while there are only 2 under-coordinated atoms around each defective atom for a double vacancy, as shown in Fig. 1(b). According to Eq. (6), the rate of phonon scattering by the 2-coordinated carbon atoms near the double vacancies at the same defect density x is given as,

$$\tau_{A,\lambda}^{-1} = \begin{cases} 4.24x\Omega\dfrac{\omega^3}{v_\lambda^2} & \lambda = LA, TA \\ 2.12x\Omega\dfrac{\omega^2}{\alpha} & \lambda = ZA \end{cases} \quad (13)$$

where the defect density x is defined as the number of defected atoms divided by the total atom number in pristine graphene. The rate of phonon scattering by the 2-coordinated carbon atoms near the single vacancies is as 1.5 times as that near the double vacancies at the same defect density. Therefore, the single vacancy defective graphene possesses the lower thermal conductivity than the double vacancy defective one. For example, for graphene flakes with 0.1% defected atoms, for single vacancy defective graphene, κ/κ_0 is 0.19, while for double vacancy defective graphene, κ/κ_0 is 0.23. Thus under the same defected atom density, single-vacancy can result in larger reduction in thermal conductivity with respect to double-vacancy defects. This explains the phenomenon observed by molecular dynamics simulations[29,51].

In summary, we find a new phonon scattering mechanism which is the scattering by the under-coordinated atoms near the vacancies. This mechanism origins from the increase of force constant of bonds associated with vacancies. The scattering of phonons by the under-coordinated atoms near the vacancies is negligible in bulk materials. However, because of the low coordination number, this mechanism has dominant effect on the phonon transport in two-dimensional vacancy defective materials. This finding is helpful not only to understand the severe suppression of thermal conductivity by vacancies, but also to apply phononic engineering to manipulate thermal conductivity in two-dimensional materials.

Methods

According to the linearized phonon Boltzmann transport equation within relaxation time approximation, the thermal conductivity in branch λ of single layer graphene (SLG) in the y direction (the longitudinal direction of graphene ribbon) is derived as:

$$\kappa_\lambda = \frac{S}{(2\pi)^2}\int c_{ph} v_{\lambda,y}^2 \tau_\lambda d\vec{q} \tag{14}$$

where S is the area of the sample, $v_{\lambda,y}$ is the y component of the group-velocity vector in branch λ ($\lambda = LA, TA$ *and* ZA, only acoustic branches are considered[49,52]), τ_λ is the averaged phonon relaxation time between successive scattering events, $\vec{q}$ is the wave vector, and c_{ph} is the volumetric specific heat of each mode, which is given as:

$$c_{ph} = \frac{k_B}{S\delta}\frac{(\hbar\omega/k_BT)^2 e^{\hbar\omega/k_BT}}{(e^{\hbar\omega/k_BT}-1)^2} \tag{15}$$

where k_B is the Boltzmann constant, $\delta = 0.335\ nm$ is the thickness of graphene, $\hbar$ is the reduced Planck constant, and T is the absolute temperature.

In SLG, the LA and TA acoustic branches are linear, whereas the ZA branch shows a quadratic dependence of the frequency on the wave vector[49,53], so

$$\omega_\lambda = \begin{cases} v_\lambda q & \lambda = LA,\ TA \\ \alpha q^2 & \lambda = ZA \end{cases} \tag{16}$$

Using this dispersion and the relationship $v_\lambda = \frac{d\omega_\lambda}{dq}$, and transforming the integral of wave vector (q) to frequency (ω), we can get

$$\kappa_\lambda = \begin{cases} \frac{k_B}{4\pi\delta}\int_0^{\omega_{D,\lambda}} \frac{(\hbar\omega/k_BT)^2 e^{\hbar\omega/k_BT}}{(e^{\hbar\omega/k_BT}-1)^2}\omega\tau_\lambda d\omega & \lambda = LA,TA \\ \frac{k_B}{2\pi\delta}\int_0^{\omega_{D,\lambda}} \frac{(\hbar\omega/k_BT)^2 e^{\hbar\omega/k_BT}}{(e^{\hbar\omega/k_BT}-1)^2}\omega\tau_\lambda d\omega & \lambda = ZA \end{cases} \tag{17}$$

where $\omega_{D,\lambda}$ is the Debye frequency, which is given as

$$\omega_{D,\lambda} = \begin{cases} 2v_\lambda\sqrt{\frac{\pi}{\Omega}} & \lambda = LA,TA \\ \frac{4\pi\alpha}{\Omega} & \lambda = ZA \end{cases} \tag{18}$$

where Ω is the primitive cell area.

The total phonon scattering rate τ_λ^{-1} is the sum of $\tau_{U,\lambda}^{-1}$, $\tau_{B,\lambda}^{-1}$, $\tau_{V,\lambda}^{-1}$ and $\tau_{A,\lambda}^{-1}$, which are given as Eq. (8–12) respectively. For a flat graphene sheet lying in the x-y plane, the reflection symmetry requires that the Hamiltonian be invariant under $z \rightarrow -z$[54]. Seol *et al.* obtained a selection rule for three-phonon scattering, which requires that an even number of ZA phonons is involved in each process. This selection rule is adopted in our calculation.

The normalized accumulative distribution of thermal conductivity is defined as,

$$F(\omega) = \frac{\kappa_{LA}(\omega)+\kappa_{TA}(\omega)+\kappa_{ZA}(\omega)}{\kappa_{LA}+\kappa_{TA}+\kappa_{ZA}} \tag{19}$$

where $\kappa_\lambda(\omega)$ is given as,

$$\kappa_\lambda(\omega) = \begin{cases} \frac{k_B}{4\pi\delta}\int_0^{\omega} \frac{(\hbar\omega/k_BT)^2 e^{\hbar\omega/k_BT}}{(e^{\hbar\omega/k_BT}-1)^2}\omega\tau_\lambda d\omega & \lambda = LA,TA \\ \frac{k_B}{2\pi\delta}\int_0^{\omega} \frac{(\hbar\omega/k_BT)^2 e^{\hbar\omega/k_BT}}{(e^{\hbar\omega/k_BT}-1)^2}\omega\tau_\lambda d\omega & \lambda = ZA \end{cases} \tag{20}$$

1. Dubi, Y. & Ventra, M. D. Heat flow and thermoelectricity in atomic and molecular junctions. *Rev. Mod. Phys.* **83**, 131–155 (2011).
2. Yang, N., Xu, X. F., Zhang, G. & Li, B. W. Thermal transport in nanostructures. *AIP Advances.* **2**, 041410 (2012).
3. Liu, S., Xu, X. F., Xie, R. G., Zhang, G. & Li, B. W. Anomalous heat conduction and anomalous diffusion in low dimensional nanoscale systems. *Eur. Phys. J. B* **85**, 337 (2012).
4. Freedman, J. P., Leach, J. H., Preble, E. A., Sitar, Z., Davis, R. F. & Malen, J. A. Universal phonon mean free path spectra in crystalline semiconductors at high temperature. *Sci. Rep.* **3**, 2963 (2013).
5. Balandin, A. A. Thermal properties of graphene and nanostructured carbon materials. *Nature. Mater.* **10**, 569–581 (2011).
6. Sadeghi, M. M., Pettes, M. T. & Shi, L. Thermal transport in graphene. *Solid State Commun.* **152**, 1321–1330 (2012).
7. Pop, E., Varshney, V. & Roy, A. K. Thermal properties of graphene: Fundamentals and applications. *MRS Bull.* **37**, 1273–1281 (2012).
8. Shahil, K. M. F. & Balandin, A. A. Thermal properties of graphene and multilayer graphene: Applications in thermal interface materials. *Solid State Commun.* **152**, 1331–1340 (2012).
9. Li, N. *et al.* Colloquium: Phononics: Manipulating heat flow with electronic analogs and beyond. *Rev. Mod. Phys.* **84**, 1045–1066 (2012).
10. Yang, N., Zhang, G. & Li, B. Thermal rectification in asymmetric graphene ribbons. *Appl. Phys. Lett.* **95**, 033107 (2009).
11. Hu, J., Ruan, X. & Chen, Y. P. Thermal Conductivity and Thermal Rectification in Graphene Nanoribbons: A Molecular Dynamics Study. *Nano Lett.* **9**, 2730–2735 (2009).
12. Zhang, G. & Zhang, H. Thermal conduction and rectification in few-layer graphene Y Junctions. *Nanoscale.* **3**, 4604–4607 (2011).
13. Sevincli, H., Sevik, C., Cagin, T. & Cuniberti, G. A bottom-up route to enhance thermoelectric figures of merit in graphene nanoribbons. *Sci. Rep.* **3**, 1228 (2013).
14. Chen, X. B., Tian, F. Y., Persson, C., Duan, W. H. & Chen, N.-X. Interlayer interactions in graphites. *Sci. Rep.* **3**, 3046 (2013).
15. Mu, X., Wu, X. F., Zhang, T., Go, D. B. & Luo, T. F. Thermal Transport in Graphene Oxide – From Ballistic Extreme to Amorphous Limit. *Sci. Rep.* **4**, 3909 (2014).
16. Tian, H. *et al.* A novel solid-state thermal rectifier based on reduced graphene oxide. *Sci. Rep.* **2**, 523 (2012).
17. Liu, X. J., Zhang, G., Pei, Q. X. & Zhang, Y. W. Phonon thermal conductivity of monolayer MoS_2 sheet and nanoribbons. *Appl. Phys. Lett.* **103**, 133113 (2013).
18. Li, W., Carrete, J. & Mingo, N. Thermal conductivity and phonon linewidths of monolayer MoS_2 from first principles. *Appl. Phys. Lett.* **103**, 253103 (2013).
19. Cai, Y. Q., Lan, J. H., Zhang, G. & Zhang, Y. W. Lattice vibrational modes and phonon thermal conductivity of monolayer MoS_2. *Physical Review B* **89**, 035438 (2014).
20. Sun, C. Q. Relaxation of the Chemical Bond. Vol. **108** *Springer Series in Chemical Physics* 795. (Berlin: Springer press, 2014).
21. Zhang, G. & Li, B. W. Impacts of doping on thermal and thermoelectric properties of nanomaterials. *NanoScale.* **2**, 1058–1068 (2010).
22. Zhang, H., Lee, G. & Cho, K. Thermal transport in graphene and effects of vacancy defects. *Phys. Rev. B* **84**, 115460 (2011).
23. Yamamoto, T. & Watanabe, K. Nonequilibrium Green's Function Approach to Phonon Transport in Defective Carbon Nanotubes. *Phys. Rev. Lett.* **96**, 255503 (2006).
24. Che, J., Cagin, T., Deng, W. Q. & Goddard III, W. A. Thermal conductivity of diamond and related materials from molecular dynamics simulations. *J. Chem. Phys.* **13**, 6888–6900 (2000).
25. Chen, K. Q. *et al.* Effect of defects on the thermal conductivity in a nanowire. *Phys. Rev. B* **72**, 045422 (2005).
26. Ratsifaritana, C. A. & Klemens, P. G. Scattering of phonons by vacancies. *Int. J. Thermophys.* **8**, 737–750 (1987).
27. Sun, C. Q. *et al.* Bond-order–bond-length–bond-strength (bond-OLS) correlation mechanism for the shape-and-size dependence of a nanosolid. *J. Phys.: Condens. Matter* **14**, 7781–7795 (2002).
28. Sun, C. Q. Size dependence of nanostructures: Impact of bond order deficiency. *Prog. Solid State Chem.* **35**, 1–159 (2007).
29. Haskins, J. *et al.* Control of Thermal and Electronic Transport in Defect-Engineered Graphene Nanoribbons. *ACS Nano* **5**, 3779–3787 (2011).
30. Klemens, P. G. & Pedraza, D. F. Thermal conductivity of graphite in the basal plane. *Carbon* **32**, 735–741(1994).
31. Klemens, P. G. Phonon scattering by oxygen vacancies in ceramics. *Physica B* **263–264**, 102–104 (1999).
32. Yeung, T. C. A. *et al.* Impact of surface bond-order loss on phonon dispersion relations and thermal conductivity of cylindrical Si nanowires. *Phys. Rev. B* **74**, 155317 (2006).
33. Yeung, T. C. A. *et al.* Effect of surface bond-order loss on electrical resistivity of metallic polycrystalline thin films. *Phys. Rev. B* **72**, 155417 (2005).
34. Sun, C. Q. *et al.* Dimension, Strength, and Chemical and Thermal Stability of a Single C-C Bond in Carbon Nanotubes. *J. Phys. Chem. B* **107**, 7544–7546 (2003).
35. Sun, C. Q., Li, C. M., Bai, H. L. & Jiang, E. Y. Melting point oscillation of a solid over the whole range of sizes. *Nanotechnology* **16**, 1290–1293 (2005).
36. Klemens, P. G. The scattering of low-frequency lattice waves by static imperfections. *Proc. Phys. Soc. A* **68**, 1113–1128 (1955).
37. Klemens, P. G. Thermal conductivity and lattice vibrational modes. *Solid State Phys.* **7**, 1–98 (1958).

38. Zhang, G. & Zhang, Y. W. Thermal conductivity of silicon nanowires: From fundamentals to phononic engineering. *Phys. Status Solidi RRL* **7**, 754–766 (2013).
39. Nika, D. L. & Balandin, A. A. Two-dimensional phonon transport in graphene. *J. Phys.: Condens. Matter.* **24**, 233203 (2012).
40. Nika, D. L., Askerov, A. S. & Balandin, A. A. Anomalous Size Dependence of the Thermal Conductivity of Graphene Ribbons. *Nano Lett.* **12**, 3238–3244 (2012).
41. Shen, Y. L. *et al.* Size and boundary scattering controlled contribution of spectral phonons to the thermal conductivity in graphene ribbons. *J. Appl. Phys.* **115**, 063507 (2014).
42. Kong, B. D., Paul, S., Nardelli, M. B. & Kim, K. W. First-principles analysis of lattice thermal conductivity in monolayer and bilayer graphene. *Phys. Rev. B* **80**, 033406 (2009).
43. Girit, C. O. *et al.* Graphene at the Edge: Stability and Dynamics. *Science* **323**, 1705–1708 (2009).
44. Grantab, R., Shenoy, V. B. & Ruoff, R. S. Anomalous strength characteristics of tilt grain boundaries in graphene. *Science* **330**, 946–8 (2010).
45. Chen, S. *et al.* Thermal conductivity of isotopically modified graphene. *Nat. Mater.* **11**, 203–207 (2012).
46. Wang, Y. *et al.* Large Thermal Conductivity Reduction Induced by La/O Vacancies in the Thermoelectric $LaCoO_3$ System. *Inorg. Chem.* **50**, 4412–4416 (2011).
47. Balandin, A. A. *et al.* Superior Thermal Conductivity of Single-Layer Graphene. *Nano Lett.* **8**, 902–907 (2008).
48. Ghosh, S. *et al.* Extremely high thermal conductivity of graphene: Prospects for thermal management applications in nanoelectronic circuits. *Appl. Phys. Lett.* **92**, 151911 (2008).
49. Nika, D. L., Pokatilov, E. P., Askerov, A. S. & Balandin, A. A. Phonon thermal conduction in graphene: Role of Umklapp and edge roughness scattering. *Phys. Rev. B* **79**, 155413 (2009).
50. Lindsay, L., Broido, D. A. & Mingo, N. Flexural phonons and thermal transport in graphene. *Phys. Rev. B* **82**, 115427 (2010).
51. Zhang, Y. Y. *et al.* Thermal conductivity of defective graphene. *Phys. Lett. A* **376**, 3668–3672 (2012).
52. Munoz, E., Lu, J. & Yakobson, B. I. Ballistic Thermal Conductance of Graphene Ribbons. *Nano Lett.* **10**, 1652–1656 (2010).
53. Kong, B. D., Paul, S., Nardelli, M. B. & Kim, K. W. First-principles analysis of lattice thermal conductivity in monolayer and bilayer graphene. *Phys. Rev. B* **80**, 033406 (2009).
54. Seol, J. H. *et al.* Two-Dimensional Phonon Transport in Supported Graphene. *Science* **328**, 213–216 (2010).

Acknowledgments

This work was financially supported by National Natural Science Foundation of China (NSFC) (Grant Nos. 11275163, 11274011, 11304264), and the Ministry of Education of China (Grant No. 20110001120133).

Author contributions

G.F.X. and G.Z. established the theoretical models and supervised the project, G.F.X. and Y.L.S. performed the calculations and data analysis, G.F.X. wrote the paper, G.Z. revised the paper. X.L.W., L.W.Y., H.P.X. and J.X.Z. discussed the results.

Additional information

Competing financial interests: The authors declare no competing financial interests.

How to cite this article: Xie, G.F. *et al.* A Bond-order Theory on the Phonon Scattering by Vacancies in Two-dimensional Materials. *Sci. Rep.* **4**, 5085; DOI:10.1038/srep05085 (2014).